Available online at www.sciencedirect.com
SCIENCE DIRECT
Surface Science 600 (2006) 2434–2442
SURFACE SCIENCE
www.elsevier.com/locate/susc

EPR properties of Au atoms adsorbed on various sites of the MgO(100) surface from relativistic DFT calculations

Cristiana Di Valentin [a], Andrea Scagnelli [a], Gianfranco Pacchioni [a,*], Thomas Risse [b], Hans-Joachim Freund [b]

[a] *Dipartimento di Scienza dei Materiali, Università di Milano-Bicocca, Via R. Cozzi, 53, 20125 Milano, Italy*
[b] *Fritz-Haber Institut der Max-Planck Gesellschaft, Department of Chemical Physics, Faradayweg 4-6, D-14195 Berlin, Germany*

Received 14 February 2006; accepted for publication 27 March 2006
Available online 4 May 2006

Abstract

Using all electron fully relativistic DFT calculations we have computed the EPR properties of Au atoms bound to various sites of the MgO surface. Changes in *g*-tensor and hyperfine coupling constants provide a way to identify the gold adsorption site and to map the surface morphology by comparison of measured and calculated EPR spectra. We found a strong reduction of the isotropic hyperfine coupling constant, a_{iso}(Au), for adsorbed gold compared to the free atom; this reduction, which is about 45% for terrace sites, is more pronounced when Au interacts with low-coordinated sites like steps, edges and corners where it is about 60%. The reduction of a_{iso}(Au) is accompanied by a corresponding increase of the superhyperfine interaction with the surface oxygen sites, as measured by $a_{iso}(^{17}O)$. Large anisotropies in the *g*-tensor are computed for all sites.

Keywords: Au atom; MgO; Electron paramagnetic resonance; DFT calculations; Hyperfine coupling constants; *g*-Tensor

1. Introduction

Thanks to spectacular advances in surface science and surface chemistry techniques, it is possible nowadays to prepare in a controlled way assemblies of atoms on "inert" supports and manipulate them at the atomic scale. Examples of chemistry on single metal atoms have been reported [1–5], showing also that modifications of the chemical activity are possible by stabilizing the metal atoms at specific defects of the surface [1]. This activity opens stimulating perspectives in the field of nanotechnology. Using an STM tip it has been possible to selectively charge Au atoms deposited on NaCl thin films [6]; in a different experiment the deposition of Au atoms on Al_2O_3 ultra-thin films grown on NiAl(110) leads to peculiar nano-structures [7]; etc. One general problem connected to this research area is the characterization of the electronic properties of the supported metal atoms. Indirect information can be obtained from adsorption of CO molecules and from the measurement of their vibrational shift, but some care is required in the interpretation of the results [8]. Few examples of direct measurements of optical transitions have also been reported, showing the importance of a combined theoretical–experimental approach for the assignment of the observed absorption bands [9,10].

A very powerful technique to study properties of isolated atoms on a support is electron paramagnetic resonance (EPR), provided that the atom possesses unpaired electrons. This technique is usually employed on polycrystalline materials with high-surface area, like for instance MgO powders. Using this technique, the group of Giamello has been able to identify the properties of isolated alkali metal atoms adsorbed on MgO powders [11–15]. Recently, it has been found that K atoms are stabilized at specific morphological sites of MgO, the reverse corners, where

* Corresponding author. Tel.: +39 02 6448 5219; fax: +39 02 6448 5403.
E-mail address: gianfranco.pacchioni@mater.unimib.it (G. Pacchioni).

0039-6028/$ - see front matter © 2006 Elsevier B.V. All rights reserved.
doi:10.1016/j.susc.2006.03.048

they are sufficiently strongly bound to survive up to 380 K [16]. Above this temperature diffusion and aggregation processes take place. The MgO surface acts as a kind of ''solvent'' which perturbs the spin properties of the adsorbed K atom, and its hyperfine coupling constants (hfcc) deviate strongly from that of the free atom. In particular, the isotropic constant, a_{iso}, is reduced by 50% when K is adsorbed on a reverse corner [16], despite the fact that no charge transfer, nor s-to-p hybridization occur, at variance with the usual interpretation of changes in a_{iso} by formation of new bonds in chemical compounds [17]. DFT calculations have been of key importance to unravel the origin of these effects. In general, the combined use of EPR measurements and ab initio calculations represents a very useful approach to characterize the properties of paramagnetic species in inorganic materials [18,19].

A similar analysis of EPR results obtained under UHV conditions using a thin MgO film prepared by chemical vapor deposition is considerably more difficult. Here the advantage is the absence of impurities in the oxide support and the atomistic control of the surface morphology thanks to the possibility to use scanning tunneling microscopy (STM) for the characterization of the top layer of the film [20]. The price to pay, however, is a considerable loss in EPR signal intensity as the surface area at disposal is strongly reduced, from hundreds of m^2/g of powder samples, to 1–2 cm^2 in the thin film regime. With a typical amount of 1 g of powder material this corresponds to an intensity ratio of approximately 10^6 in favor of the powder assuming equivalent coverage. The detection limit of X-band EPR equipment renders the minimal number of paramagnetic centers for this class of species to be approximately 10^{12} spins. However, this is sufficient to collect well resolved EPR spectra for paramagnetic defects [20] or paramagnetic atoms adsorbed on thin, single crystalline MgO films grown on Mo(100) [21] as reported recently. The study of deposited Au atoms at very low temperature (30 K) has unambiguously shown adsorption on top of oxygen anions of the MgO(100) terraces [21]. Changes of the order of 50% have been observed in the a_{iso} value of the adsorbed Au atom, in analogy with the results for K on MgO powders [16], despite the fact that different adsorption sites have been identified (flat terraces for Au and reverse corners for K).

These experimental studies open various questions for theory. In fact, in both studies the role of the calculations has been important to provide a theoretical frame to explain the observed reduction of a_{iso}. In fact, the EPR properties of atoms such as K and Au are very sensitive probes for the interaction with different surface sites. Depending on the experimental conditions it should be possible to populate a variety of different adsorption sites. A theoretical mapping of the EPR properties is important to properly identify the sites as well as to understand the details of the metal–oxide interaction. This is even more important when the bonding involves defect centers like for instance oxygen vacancies or divacancies. This mapping, which has been reported for K on MgO [16], does not exist for Au, and is the subject of the present paper. A difficulty connected to the theoretical treatment of Au, not present with K, is that relativistic effects are essential and need to be included explicitly.

The present paper reports calculations of the bonding properties of Au on various sites of MgO (position, binding energy, etc.) and of the corresponding EPR properties, hyperfine coupling constants (both isotropic and dipolar parts) and *g*-tensors. To this end we have performed cluster model calculations of the Au/MgO interaction using two different codes: Gaussian03 (G03) [22] for geometry optimizations and Amsterdam Density Functional (ADF) [23–26] for all electron relativistic calculation of the spin properties. The results provide a basis for future interpretation of experimental EPR results on MgO substrates decorated by Au atoms.

2. Details of calculations

The calculations have been performed at the DFT level using embedded cluster models. For geometry optimizations we used the G03 code [22] and the gradient-corrected B3LYP [27,28] and PW91 [29] exchange-correlation functionals. For these calculations we used a scalar relativistic effective core potential (ECP) for Au. For this ECP the $5s^25p^65d^{10}6s^1$ electrons are treated explicitly as valence electrons (19-electron ECP [30]). The use of an ECP on Au does not allow to compute the hyperfine coupling constants (hfcc) for this nucleus. This is done using the ADF code (see below). The *g*-values have been evaluated in selected cases with G03 using the spin–orbit perturbation scheme of Neese [31]. The Mg and O atoms of the support have been treated at the all electron level using a 6–31 G* GTO basis sets [32] (6–31 G on the Mg atoms second neighbors of Au). The MgO clusters have been embedded in point charges (PC) and ECPs with no associated basis functions to provide a simple representation of the finite size of the Mg cations at the interface between the cluster and the PCs (these atoms are indicated as Mg^*). We also tested a simplified embedding approach where the MgO cluster is embedded only in a set of PCs since this is the method used in the ADF calculations. In this case, to avoid possible artifacts due to the absence of interface Mg^* atoms, we have carefully checked the results versus the size of the MgO cluster. In the geometry optimizations the Au atom and the nearest neighbor O atoms are free to move, the rest being fixed at truncated bulk positions.

The EPR properties have been determined at the all electron relativistic level using the zero order regular approximation (ZORA) [33–37] to the Dirac equation as implemented in the ADF code [23–26]. The calculations have been performed using the PW91 functional (hybrid functionals are not implemented in ADF) using large STO basis sets: uncontracted [23s15p11d5f] basis for Au [36]; uncontracted [7s4p1d] and [5s3p1d] basis sets for Mg and O, respectively.

The use of clusters embedded in PCs in the ADF code does not allow a full geometry optimization and therefore the search for the optimal structure was done using the G03 code. The determination of the EPR parameters has been done by performing a single point calculation at the optimal geometry obtained with G03 (PW91 functional). In the case of adsorption on a terrace we have verified that practically the same adsorption properties were obtained by performing a point-by-point optimization with ADF. Using both G03 and ADF codes, we performed a careful analysis of the dependence of the results on: (a) cluster size, (b) embedding procedure (simple embedding in PCs or in PCs and ECPs), (c) basis set of Au, (d) exchange-correlation functional (B3LYP, PW91, or other functionals). The results, not reported in full detail, show a remarkable stability, in particular as far as the adsorption geometry is concerned. As it will be discussed below, this is the most important ingredient for the determination of the hfcc's. In the following we report only hfcc's obtained with the largest MgO clusters used.

The hyperfine spin-Hamiltonian, $\mathbf{H_{hfc}} = \mathbf{S}\cdot\mathbf{A}\cdot\mathbf{I}$, is given in terms of the hyperfine matrix **A** which describes the coupling between the electron and the nuclear spins [38]. The components of **A** can be represented as the sum of an isotropic part, a_{iso}, related to the Fermi contact term, and the matrix **B** which represents the "classical" dipolar interaction between two magnetic (electron and nuclear) moments. Typical anisotropic interactions can be observed when the unpaired electron is in directional orbitals like p, d, f, etc. The **A** tensor can therefore be represented in matrix notation as $\mathbf{A} = a_{iso}\mathbf{1} + \mathbf{B}$. The hyperfine interactions of the electron spin with the nuclear spin of the ^{197}Au and ^{17}O nuclides have been determined at two levels. In the first case we performed spin-polarized scalar relativistic calculations without spin–orbit coupling (SR). In the second case spin–orbit effects (SO) are included explicitly and the calculations are done using spin-restricted density functional [36].

The quality of the relativistic approach and of the basis set on Au can be verified by computing the hfcc of the free atom, Table 1. At the SR level (PW91 functional) $a_{iso} = 1069$ G is very close to the experimental value for the gas-phase atom, 1089 G [39,40]. PBE [41] or BLYP [42,28] functionals provide similar answers, Table 1. The inclusion of spin–orbit coupling has only a moderate effect on a_{iso} which goes from 1069 G (SR) to 1076 G (SO), Table 1. These results reproduce those described in Ref. [36]. However, in comparing calculated and experimental hfcc's, one has to keep in mind some approximations in the theoretical approach. First of all, we considered a point nuclear model. It has been reported that the use of a more realistic finite size of the Au nucleus can have the effect to reduce the hfcc by about 13% [43]. In general, the quantitative calculation of hfcc's for transition metal systems is still a challenge to quantum chemistry. Core-shell spin polarization and spin contamination effects contribute to intrinsic uncertainties [44]. Furthermore, small changes are connected to the choice of the exchange-correlation functional. For all these reasons, an agreement of computed versus measured values of the isotropic part of the hfcc's of 10–15% has to be considered as satisfactory.

Table 1
Isotropic hyperfine coupling constant (in G) of gas-phase Au atom[a]

	SR	SO
PW91	1061	1076
PBE	1115	1097
BLYP	1063	1049
Exp.	1089 [39,40] 1180–1120 [58]	

[a] SR = scalar relativistic, SO = spin–orbit; results obtained with the ZORA approach.

3. Results and discussion

3.1. Au/MgO adsorption properties

The optimal geometry and adsorption energy, E_a, of Au atoms on various sites of the MgO surface are reported in Table 2. The E_a values are not corrected by the basis set superposition error and, therefore, are slightly overestimated. Beside the flat (100) terraces, we considered edge, step, double step, corner and reverse corner sites, see Fig. 1. We also considered Au adsorption on a point defect like an oxygen vacancy, or F center [45]. The adsorption of Au on flat terraces has been addressed also in other theoretical studies, using periodic supercell calculations and plane wave basis sets [46–48] or cluster models and atomic orbital basis sets [49,50]. It represents therefore a good test of the approach used here. Au binds to a five-coordinated O anion, O_{5c}, with a binding energy of 1.20 eV (PW91) or 0.77 eV (B3LYP). The relatively large difference in E_a with the two functionals is not surprising as it is well known that the adsorption energies of metal atoms on oxide surfaces depend quite strongly on the exchange-correlation func-

Table 2
Computed adsorption energy, E_a, and Au–O equilibrium bond distance, r_e, for a Au atom adsorbed on various sites (see Fig. 1) of the MgO surface (G03 results)

MgO site	Cluster	PW91		B3LYP	
		E_a,[a] eV	r_e, Å	E_a,[a] eV	r_e, Å
Terrace	$O_9Mg_9Mg^*_{16}$	1.20	2.298	0.77	2.339
Edge	$O_{10}Mg_{10}Mg^*_{14}$	1.34	2.240	0.99	2.259
Step	$O_{12}Mg_{12}Mg^*_{17}$	1.52	2.310	1.09	2.276
Double step	$O_{12}Mg_{12}Mg^*_{18}$	1.56	2.469	1.13	2.377
Corner	$O_4Mg_4Mg^*_6$	1.48	2.186	1.20	2.206
Reverse corner	$O_{11}Mg_{11}Mg^*_{18}$	2.01	2.474/2.726	1.41	2.474, 2.946
F center	$O_{20}Mg_{21}Mg^*_{16}$	3.30	2.858[a]	2.89	2.875[b]

[a] The E_a values are not corrected by the basis set superposition error and, therefore, are slightly overestimated.
[b] Distance from the nearest Mg cation.

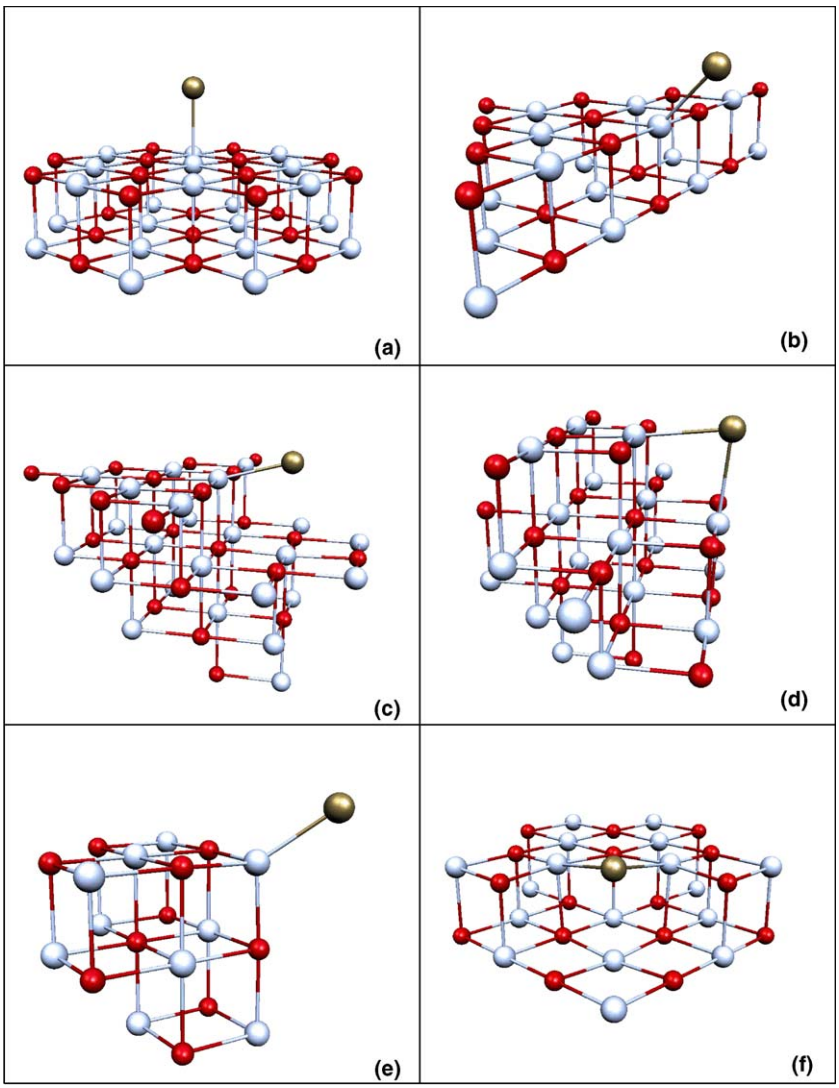

Fig. 1. Optimal geometry of a Au atom adsorbed on various sites of the MgO surface. (a) Terrace; (b) edge; (c) step; (d) double step; (e) corner; (f) reverse corner.

tional used [51]. According to our experience, among gradient-corrected functionals, B3LYP and PW91 provide a lower and an upper bound to the adsorption energy of metal atoms on MgO, respectively. Both functionals indicate a significant bond strength, of the order of 1 eV, much higher than that of an atom like K to the same site (0.20 eV at the B3LYP level [16]). On the other hand, the Au–O distance, about 2.3 Å, varies only slightly with the functional used, Table 2 and Fig. 1(a). The changes in geometry with the size of the cluster are very small. The results are close to those obtained using a periodic approach [46] where it was found that Au binds with a distance of 2.276 Å and a binding energy of 0.89 eV (PW91 results) to the surface oxygen. The difference in binding energy between cluster and periodic models using the same PW91 functional must be ascribed to the occurrence of the basis set superposition error in the former case. Other theoretical studies give a O–Au distance which goes from a minimum of 2.24 Å to a maximum of 2.34 Å and a binding energy which, depending on the exchange-correlation functional, goes from 0.74 to 1 eV [46–50]. The distance of Au from the O_{5c} anion of the MgO(100) surface has been optimized also by points using the ADF code and two cluster models, O_9Mg_9 and $O_{21}Mg_{21}$, embedded in PCs. No relaxation of the substrate is allowed in this case. At the SR level the distance is 2.322 ± 0.001 Å. The results are very close to those obtained with G03 using an ECP for Au and a full geometry optimization.

The binding energy of Au increases when the interaction involves other sites, in particular low-coordinated anions. On an edge site, Fig. 1(b), the bonding is slightly stronger than on a terrace, being 1.34 eV (PW91) or 0.99 eV (B3LYP); this corresponds also to a reduction of the O–Au distance of 0.06–0.08 Å, Table 2. On this site gold interacts with only one oxygen. On a mono-atomic step, beside the interaction with the O_{4c} ion, there is also interaction with the O_{5c} anion of the basal plane, Fig. 1(c). This leads to a small increase of the binding energy (1.52 eV at the

PW91 level and 1.09 eV with B3LYP), which is not accompanied by a shortening of the O_{4c}–Au distance, Table 2. The bond strength on a step is very similar to that found on a double step, Fig. 1(d), where Au binds simultaneously to two equivalent O_{4c} ions; in this case the O–Au distance is considerably larger than on a step, and even larger than that of the terrace sites, Table 2. A three-coordinated oxide anion of a corner, O_{3c}, exhibits a O–Au bond strength similar to that of step and double-step sites, but a much shorter equilibrium distance which reaches the shortest value among the cases considered here, 2.19–2.20 Å, Table 2 and Fig. 1(e). We will see below that this leads also to the largest reduction of a_{iso}(Au). The last site considered is a reverse corner, Fig. 1(f), where Au binds simultaneously to two O_{4c} and to one O_{5c} anion. This leads to a considerably higher binding energy, 2.0 eV in PW91 and 1.41 eV in B3LYP. The reverse corner is therefore the most stable adsorption site, in full analogy with what found for K/MgO [16]. On this site the Au atom is equi-distant from the two O_{4c} atoms, with O–Au separations of about 2.47 Å, and a longer distance from O_{5c}, 2.73 Å, Fig. 1(f).

Completely different is the bonding of a Au atom to a neutral oxygen vacancy (F_s^0). Here the bond strength is of 2.9 eV (B3LYP) or 3.3 eV (PW91), and the Au atom is close to the Mg cations of the vacancy. The details of this interaction such as the bond strength or the partial charge transfer from the F center to gold, etc. have been described elsewhere [46]. Here we are only interested in the optimal geometry to be used in the determination of the hfcc's and *g*-tensors.

3.2. Hyperfine coupling constants

The computed spin population and hfcc's of Au/MgO are collected in Table 3. We start our discussion with the terrace sites. At the equilibrium Au–O distance (computed with G03), a_{iso} is strongly reduced from the gas-phase value: 591.8 G at the SR level and 608.1 G after inclusion of spin–orbit effects. Performing a point-by-point optimization at the SR level a_{iso}(Au) is practically the same, 604 G [21]. The spin population on Au however, about 0.8, indicates that the 6s orbital of Au is singly occupied and that little charge transfer has occurred upon adsorption. The fact that the inclusion of SO does not alter the results obtained at the SR level has already been observed for the free atom, Table 1, and applies to all cases considered, see Table 3. The computed a_{iso}(Au) corresponds to about 55% of the free atom value. This strong reduction in the isotropic component is not accompanied by an appreciable increase of the dipolar part which is 2.6–2.7 G, Table 3. These results have been obtained with a $O_{21}Mg_{21}$ cluster, but very similar are those obtained with O_9Mg_9 and $O_{13}Mg_{13}$ clusters (not reported here for brevity).

The main difference between Au and K adsorbed on MgO is that K is weakly bound on the flat MgO terraces so that its distance from the surface is long, 2.88 Å, and the reduction of a_{iso} is not very pronounced (about 20% [16]). Au is more strongly bound to MgO, by about 1 eV, Table 2, and its distance from the surface is comparatively shorter, so that also the effect on a_{iso} is larger. In fact, there is a direct, almost linear relationship between a_{iso}(Au) and

Table 3
Adsorption energy and hyperfine coupling constants of Au atoms adsorbed on regular and low-coordinated sites of the MgO surface[a]

Site	Cluster	E_a, eV		Spin density	^{197}Au		^{17}O	
					a_{iso}, G	B_1, B_2, B_3, G	a_{iso}, G	B_1, B_2, B_3, G
Terrace	$O_{21}Mg_{21}$	1.01	SR	0.78	591.8	−2.7, −2.7, 5.4	−39.4	11.1, 11.1, −22.2
		0.91	SO	–	608.1	−2.6, −2.6, 5.2	−29.7	13.5, 13.5, −27.0
Edge	$O_{10}Mg_{10}$	1.18	SR	0.77	492.8	−4.4, −2.5, 6.9	−49.7	12.4, 12.4, −24.8
		1.19	SO	–	508.7	−3.2, −4.3, 7.5	−37.0	15.6, 16.4, −32.0
Step	$O_{24}Mg_{24}$	1.51	SR	0.71	501.0	−4.3, −0.7, 5.0	−36.3	11.6, 11.6, −23.2
		1.56	SO	–	506.0	−3.6, −2.8, 6.4	−25.4	12.7, 14.9, −27.6
Double step	$O_{20}Mg_{20}$	1.49	SR	0.76	538.7	−3.6, 0.7, 2.9	−25.9	7.4, 7.4, −14.8
		1.44	SO	–	524.8	−2.6, −3.3, 5.9	−20.8	6.3, 9.3, −15.6
Corner	$O_{10}Mg_{10}$	1.31	SR	0.78	410.5	−4.1, −4.1, 8.2	−56.0	10.4, 10.4, −20.8
		1.32	SO	–	418.5	−3.9, −3.9, 7.8	−45.1	13.7, 13.7, −27.4
Reverse corner	$O_{17}Mg_{17}$	1.78	SR	0.75	552.6	−2.1, −1.4, 3.5	−15.7[b]	4.2, 4.2, −8.4[b]
							−10.5[c]	3.9, 3.9, −7.8[c]
		1.87	SO	–	542.9	−2.9, −0.3, 3.2	−14.7[b]	3.2, 4.4, −7.6[b]
							−9.3[c]	3.1, 3.9, −7.0[c]
F center	$O_{20}Mg_{21}$	3.17	SR	0.36	156.3	−2.5, −2.5, 5.0	–	–
		3.20	SO	–	159.3	−12.5, −12.5, 25.0	–	–

[a] Results obtained by performing a single point calculations on the optimal geometry obtained at PW91 level with G03, see Table 2. The E_a values are not corrected by the basis set superposition error and, therefore, are slightly overestimated.
[b] Values for the O_{4c} ions of the reverse corner, see Fig. 1(f).
[c] Values for the O_{5c} ion of the reverse corner, see Fig. 1(f).

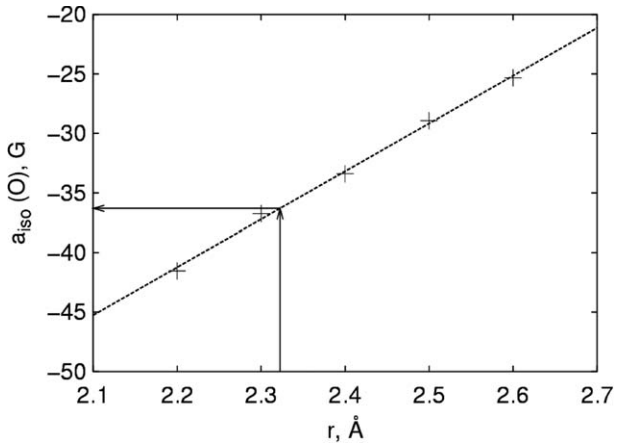

Fig. 2. Dependence of the isotropic hyperfine coupling constant of the surface O_{5c} terrace ion on the O–Au distance, r (Å). The results refer to the $O_{21}Mg_{21}$ cluster. The arrows indicate the position of the lowest energy configuration.

the surface distance [21]: shorter O–Au distances correspond to smaller a_{iso}(Au) values. This implies also that small errors in the computed adsorption distance will reflect in similar uncertainties in the predicted a_{iso}.

The large reduction of a_{iso}(Au) is a direct consequence of the interaction with the oxygen atom of the surface. The spin density is polarized away from the surface to reduce the Pauli repulsion and partially delocalized over the oxide anion. The use of the ^{17}O isotope allows the determination of the superhypefine interactions [16,21]. The calculations show that the hyperfine constant on the O_{5c} surface ion is relatively large, $a_{iso}(^{17}O) \approx -30$ G at the SO level, with an important dipolar contribution, 13.5 G. Also the O_{5c} anion isotropic hfcc changes with the O–Au distance in a linear way, Fig. 2. A shorter distance corresponds to a larger absolute value of $a_{iso}(^{17}O)$. This is consistent with a larger hybridization of the O and Au valence orbitals for closer contacts, with partial transfer of the spin density from Au to O.

The hfcc's for Au/MgO have recently been determined from EPR experiments on Au atoms deposited at very low temperature on MgO thin films in UHV; the experiments show that the atoms are directly on-top of the oxide anions [21]. It was found that a_{iso}(Au) is 501 G and $A_{\perp}(^{17}O) = 20$ G, in qualitative agreement with the present calculations. The accurate measurement of a_{iso}(Au) allows us to conclude that the computed value is overestimated and that there is space for improvement of the theoretical data. On the other hand, the very small dipolar part of the hfcc for both Au and O isotopes is correctly reproduced, showing that the essential ingredients of the Au–MgO interaction are properly described at this level of theory, taking into account the intrinsic limitations in the calculation of the isotropic part of the hfcc discussed above (see Section 2). The EPR signal observed in the experiments correspond to Au atoms sitting on the flat terraces of MgO [21]. A small fraction of Au atoms does also nucleate on lower coordinated sites, such as corners or edges, however, it has not been possible to detect signals arising form these sites. In this respect a knowledge of the magnetic properties of Au atoms bound to low-coordinated sites can be very valuable.

We consider first Au adsorbed on an edge site, Fig. 1(b), where the O–Au distance is slightly shorter than on the terrace, Table 2. Here a_{iso}(Au) is 492.8 G (SR) or 508.7 G (SO), i.e., considerably smaller than on a terrace. Notice that these values are in much better agreement with the experimental data than those computed for terrace sites. On the other hand, the fact that the Au atoms are on-top of O_{5c} ions on flat (1 0 0) terraces is shown unambiguously by angular dependent measurements that allow the determination of the symmetry and direction of the tensor [21]. In this respect the experimental data are of great importance to estimate the level of accuracy of the computed values. The dipolar part is very small and similar to the terrace case and will not be further discussed. The results are very similar (virtually indistinguishable) from those obtained for a step site, Fig. 1(c), a_{iso}(Au) = 501.0 G (SR) or 506.0 G (SO), Table 3. A small difference is found for $a_{iso}(^{17}O)$; in particular, this is larger for the edge than for the step site (−37 G versus −25 G at SO level, Table 3). The reason is that while on an edge site Au interacts with just one O_{4c} anion, Fig. 1(b), on a step there is a weak interaction also with a O_{5c} anion of the basal plane, Fig. 1(c), and the spin density is distributed over two O anions (the second $a_{iso}(^{17}O)$ is small, −6.7 G).

On a double step, Fig. 1(d), Au interacts simultaneously with two O_{4c} ions and the O–Au distance increases to 2.47 Å, Table 3. Compared to edge or step sites a_{iso}(Au) is slightly larger, 538.7 G (SR) or 524.8 G (SO). The smallest value of a_{iso}(Au), 400 G, Table 3, is found for a corner site, O_{3c}, where the O–Au distance becomes 2.19 Å. Not surprisingly, $a_{iso}(^{17}O)$ increases in absolute value and becomes −45 G (SO). On a reverse corner, Fig. 1(f), the O_{4c}–Au distance is similar to that found on a double step and a_{iso}(Au) is also comparable, 553 G (SR) or 543 G (SO), i.e., it is only slightly reduced compared to a terrace site. This is different from the case of K/MgO where going from adsorption on a terrace to a reverse corner the reduction with respect to the free atom goes from ≈20% to ≈50% [16].

The last case considered is that of a neutral F^0 center. The adsorption of a Au atom on this diamagnetic defect leads to a paramagnetic center. We have considered only the F center located at the flat terraces of MgO despite the fact that F centers form preferentially on low-coordinated sites, like steps or edges [20,52]. The F center is a strong binding site for Au and other metal atoms [46]. The computed EPR properties are indicative of an unusual interaction. a_{iso}(Au) is drastically reduced, 156 G (SR) or 159 G (SO), without increasing the dipolar part, Table 3. This strong reduction can be attributed to a charge transfer from the F center to the Au atom, which becomes negatively charged, with transfer of the spin density towards

the vacancy. A closer inspection shows that the spin population on Au is 0.36 only, and is mainly on a p_z orbital normal to the surface, not on the 6s orbital. This explains the large reduction of a_{iso} and the corresponding increase of the dipolar part, in particular at SO level, see Table 3. The rest of the spin is localized in the vacancy. This results in a hyperfine interaction with the Mg cation at the bottom of the vacancy (second layer of the MgO surface), $a_{iso}(^{25}Mg) = -12.5$ G (SR) or -10.5 G (SO). The interaction with the four Mg ions in the top layer is smaller, $a_{iso}(^{25}Mg) \cong -4$ G at both SR and SO levels. With respect to a paramagnetic F^+ center computed at the same level for a truncated bulk geometry, there is a small increase of the hyperfine coupling with the apical Mg ion (-2.7 G) while the value for the four Mg ions at the surface, -5.3 G, is similar. The similarity of the ^{25}Mg hyperfine constants in Au/F(MgO) and F^+(MgO) suggests that the electronic structure of the surface complex can be described as Au^-/F^+(MgO) and is a proof of the occurrence of a charge transfer.

3.3. g-Tensor

We first consider the computed *g*-tensor for Au bound on terrace sites using different methods and models. For this system well defined experimental data are available [21]. This allows a direct comparison of this delicate quantity. The results show a strongly anisotropic *g*-tensor, but the values change as function of the theoretical treatment. The size of the cluster has little effect on the *g*-tensor: the values calculated with ZORA and O_9Mg_9 and $O_{21}Mg_{21}$ clusters differ on the third decimal place, Table 4. Also the DFT functional, although important, does not change dramatically the values of the *g*-tensor: PW91 and B3LYP results obtained with G03 on O_9Mg_9 clusters are similar, Table 4. The largest difference is found when G03 and ZORA values are compared using the same cluster, exchange-correlation functional, and geometry (see O_9Mg_9 results in Table 4): the G03 values are much larger than those obtained with ZORA. These latter are reasonably close, given the approximations of the method, to the experimental ones: $g_\parallel = 1.9680$, $g_\perp = 2.0760$ (ZORA) versus $g_\parallel = 1.9904$, $g_\perp = 2.0652$ (exp.) [21]. The better evaluation of the *g*-tensor at the ZORA level is not unexpected. In fact, differently from most approaches where the *g*-tensor is calculated by means of second order perturbation theory and the spin–orbit effect is included only in first order [31], in ZORA spin–orbit is treated variationally [37]. This is particularly important in situations of near orbital degeneracy where a perturbative treatment becomes unreliable. Even with ZORA however the difference between computed and experimental values is relatively high, being on the second decimal place. This, together with the previous discussion suggests that the values of the *g*-tensors provide at best a qualitative and certainly not a quantitative estimate of the experimental values.

With this in mind we have computed the *g*-tensors for Au atoms adsorbed on various sites of the MgO surface, Table 4. In some cases we compare the ZORA results with G03 calculations performed with the same PW91 functional. For all adsorption sites the *g*-values are much more shifted with respect to the free electron value than for the terrace. Most sites exhibit an orthorhombic signal, with the exception of the corner site where the signal is uniaxial, Table 4. The tendency of G03 to give much larger values than ZORA is confirmed for all sites considered.

We also considered Au atoms adsorbed on a neutral F center. We have seen above that this is a special bonding interaction. With G03 (PW91) $g_\parallel = 1.9475$ and $g_\perp = 2.0043$, two values close to those obtained with B3LYP, $g_\parallel = 1.9506$, $g_\perp = 2.0048$, Table 4. The axial component is below the free electron value while the perpendicular one is above it. These values differ completely from those obtained with ZORA: $g_\parallel = 1.93207$, and $g_\perp = 1.58308$, Table 4. Such a large deviation from the free electron value, and the strong discrepancy with the G03 value, cast serious doubts on the calculation of this quantity. We have seen above that in principle ZORA performs better in situations of near orbital degeneracy and for heavy atoms [31,37]. On the other hand, ZORA does not include spin polarization which is expected to improve the results. The reasons for the large discrepancy between G03 and ZORA in the calculation of the *g*-tensor for Au adsorbed on a neutral F center of MgO, are not yet clear.

This discussion shows how delicate the calculation of *g*-factors is for heavy elements where spin–orbit coupling is important. In fact, the theory underlying this property is still under development, and new methods are presently under investigation [53–57].

Table 4
g-Values of Au atoms adsorbed on regular and low-coordinated sites of the MgO surface[a]

Site	Cluster	Method	g_1, g_2, g_3
Terrace	O_9Mg_9	G03 (PW91)	2.1297, 2.1297, 2.0077
		G03 (B3LYP)	2.1219, 2.1219, 2.0080
		ZORA (PW91)	2.0739, 2.0739, 1.9706
	$O_{21}Mg_{21}$	ZORA (PW91)	2.0759, 2.0759, 1.9680
	MgO	Exp. [21]	2.0652, 2.0652, 1.9904
Edge	$O_{10}Mg_{10}$	G03 (PW91)	2.1553, 2.1483, 2.0092
		ZORA (PW91)	2.0970, 2.0818, 1.9659
Step	$O_{24}Mg_{24}$	ZORA (PW91)	2.0612, 2.0501, 1.9773
Double step	$O_{20}Mg_{20}$	ZORA (PW91)	2.0644, 2.0025, 1.9893
Corner	$O_{10}Mg_{10}$	G03 (PW91)	2.2075, 2.2075, 2.0075
		ZORA (PW91)	2.1393, 2.1393, 1.9588
Reverse corner	$O_{17}Mg_{17}$	G03 (PW91)	2.1349, 2.0649, 2.0052
		ZORA (PW91)	2.1542, 2.0281, 1.9570
F center	$O_{20}Mg_{21}$	G03 (PW91)	2.0043, 1.9475, 1.9475
		G03 (B3LYP)	2.0048, 1.9506, 1.9506
		ZORA (PW91)	1.9321, 1.5831, 1.5827

[a] ZORA (SO) results obtained by performing a single point calculation on the optimal geometry obtained at PW91 level with G03, see Table 2.

4. Conclusions

We have studied the adsorption and spin properties of isolated Au atoms on various sites of the MgO surface, including oxygen vacancies. Aim of the paper is to provide a map of hyperfine coupling constants and g-tensors deduced from first principles calculations to be used in connection with experimental data for the identification of sites where the Au atoms are stabilized. Recent EPR studies on Au atoms deposited on MgO(1 0 0) thin films at very low temperature (30 K) have shown that the Au atoms are preferentially bound to the O_{5c} sites of the MgO flat terraces [21]. However, the low diffusion barrier for Au on MgO, 0.24 eV according to DFT calculations [46], suggests that at higher temperatures other more strongly binding sites will be populated to a larger extent. This is indeed the case of K atoms deposited on high-surface area MgO at RT where the K atoms are stabilized on reverse corners [16].

An effect common to both Au and K atoms is the strong reduction in the isotropic hfcc upon adsorption. Compared to the gas-phase atom, a_{iso} is reduced by about 50%. The change in isotropic hfcc is not related to the occurrence of charge transfer to or from the surface or to intra-unit s–p hybridization of the Au atom. Rather, it is due to an expansion of the outer 6s electron to reduce the Pauli repulsion with the surface, accompanied by a moderate transfer of spin density to the surface oxygen. In this work we have shown that the a_{iso} value is diagnostic of the site where gold is stabilized, although in some cases the differences are too small to allow a distinction. This could be facilitated by the combined analysis of g-tensor and hfcc's, but some care is needed in the analysis of the results as it is clear that both quantities are reproduced with some errors due to inherent approximations in the computational method.

Acknowledgements

This work has been supported by the Italian MIUR through a Cofin 2005 project and the European Project STRP GSOMEN. Computer time was provided by the CINECA computing center through the "Iniziativa di calcolo parallelo" of the Istituto Nazionale per la Fisica della Materia (INFM). G.P. thanks the A. Von Humboldt Foundation for financial support during his stay at the Fritz-Haber Institut in Berlin.

References

[1] S. Abbet, A. Sanchez, U. Heiz, W.D. Schneider, A.M. Ferrari, G. Pacchioni, N. Rösch, J. Am. Chem. Soc. 122 (2000) 3453.
[2] K. Judai, A. Wörz, S. Abbet, U. Heiz, A. Del Vitto, L. Giordano, G. Pacchioni, Phys. Chem. Chem. Phys. 7 (2005) 955.
[3] M. Bäumer, H.J. Freund, Prog. Surf. Sci. 61 (1999) 127.
[4] S. Abbet, U. Heiz, H. Häkkinen, U. Landman, Phys. Rev. Lett. 86 (2001) 5950.
[5] M. Frank, M. Bäumer, Phys. Chem. Chem. Phys. 2 (2000) 3723.
[6] J. Repp, G. Meyer, F.E. Olsson, M. Persson, Science 305 (2004) 493.
[7] M. Kulawik, N. Nilius, H.J. Freund, Phys. Rev. Lett. 96 (2006) 036103.
[8] M. Sterrer, T. Risse, H.-J. Freund, J. Carrasco, F. Illas, C. Di Valentin, L. Giordano, G. Pacchioni, Angew. Chem. 45 (2006) 2633.
[9] M.H. Schaffner, F. Patthey, W.D. Schneider, L.G.M. Pettersson, Surf. Sci. 402–404 (1998) 450.
[10] J.-M. Antonietti, M. Michalski, U. Heiz, H. Jones, K.H. Lim, N. Rösch, A. Del Vitto, G. Pacchioni, Phys. Rev. Lett. 94 (2005) 213402.
[11] E. Giamello, A. Ferrero, S. Coluccia, A. Zecchina, J. Phys. Chem. 95 (1991) 9385.
[12] D.M. Murphy, E. Giamello, J. Phys. Chem. 98 (1994) 7929.
[13] D.M. Murphy, E. Giamello, A. Zecchina, J. Phys. Chem. 97 (1993) 1739.
[14] M. Chiesa, M.C. Paganini, E. Giamello, D.M. Murphy, J. Phys. Chem. B 105 (2001) 10457.
[15] M. Chiesa, E. Giamello, M.C. Paganini, G. Pacchioni, R. Soave, D.M. Murphy, Z.J. Sojka, Phys. Chem. B 105 (2001) 497.
[16] M. Chiesa, E. Giamello, C. Di Valentin, G. Pacchioni, Z. Sojka, S. Van Doorsiaer, J. Am. Chem. Soc. 127 (2005) 16935.
[17] W. Weltner, Magnetic Atoms and Molecules, Dover, New York, 1983.
[18] D. Ricci, C. Di Valentin, G. Pacchioni, P.V. Sushko, A.L. Shluger, E. Giamello, J. Am. Chem. Soc. 125 (2003) 738.
[19] M. Chiesa, M.C. Paganini, G. Spoto, E. Giamello, C. Di Valentin, A. Del Vitto, G. Pacchioni, J. Phys. Chem. B 109 (2005) 7314.
[20] M. Sterrer, E. Fischbach, T. Risse, H.-J. Freund, Phys. Rev. Lett. 94 (2005) 186101/1.
[21] M. Yulikov, M. Sterrer, M. Heyde, H.-P. Rust, T. Risse, H.J. Freund, G. Pacchioni, A. Scagnelli, Phys. Rev. Lett. 96 (2006) 146804.
[22] M.J. Frisch et al., GAUSSIAN03, Revision A.7, Gaussian Inc., Pittsburgh, PA, 2003.
[23] E.J. Baerends et al., ADF 2004.01, http://www.scm.com/.
[24] E. van Lente, E.J. Baerends, G. Snijders, J. Chem. Phys. 101 (1994) 9783.
[25] E. van Lente, G. Snijders, E.J. Baerends, J. Chem. Phys. 105 (1996) 6505.
[26] G. te Velde, F.M. Bickelhaupt, E.J. Baerends, C. Fonseca Guerra, S.J.A. van Gisbergen, J.G. Snijders, T. Ziegler, J. Comp. Chem. 22 (2001) 931.
[27] A.D. Becke, J. Chem. Phys. 98 (1993) 5648.
[28] C. Lee, W. Yang, R.G. Parr, Phys. Rev. B 37 (1988) 785.
[29] J.P. Perdew, J.A. Chevary, S.H. Vosko, K.A. Jackson, M.R. Pederson, D.J. Singh, C. Fiolhais, Phys. Rev. B 46 (1992) 6671.
[30] P.J. Hay, W.R. Wadt, J. Chem. Phys. 82 (1985) 299.
[31] F. Neese, J. Chem. Phys. 115 (2001) 11080.
[32] R. Ditchfield, W.J. Hehre, J.A. Pople, J. Chem. Phys. 54 (1971) 724.
[33] C. Chang, M. Pelissier, P. Durand, Phys. Scr. 34 (1986) 394.
[34] J.-L. Heully, I. Lindgren, E. Lindroth, S. Lundqvist, A.-M. Martennson-Pendrill, J. Phys. B 19 (1986) 2799.
[35] E. van Lente, E.J. Baerends, G. Snijders, J. Chem. Phys. 99 (1993) 4597.
[36] E. van Lente, A. van der Avoird, P.E.S. Wormer, J. Chem. Phys. 108 (1998) 4783.
[37] E. van Lenthe, P.E.S. Wormer, A. van der Avoird, J. Chem. Phys. 107 (1997) 2488.
[38] J.A. Weil, J.R. Bolton, J.E. Wertz, Electron Paramagnetic Resonance, John Wiley & Sons, New York, 1994.
[39] G. Wessel, H. Lew, Phys. Rev. 92 (1953) 641.
[40] Y. Ting, H. Lew, Phys. Rev. 105 (1957) 581.
[41] J.P. Perdew, K. Burke, M. Ernzerhof, Phys. Rev. Lett. 77 (1996) 3865.
[42] A.D. Becke, Phys. Rev. A 38 (1988) 3098.
[43] Z.C. Zhang, N.C. Pyper, Mol. Phys. 64 (1988) 963.
[44] M. Munzarova, M. Kaupp, J. Phys. Chem. A 103 (1999) 9966.
[45] A.M. Ferrari, G. Pacchioni, J. Phys. Chem. 99 (1995) 17010.
[46] A. Del Vitto, G. Pacchioni, F. Delbecq, P. Sautet, J. Phys. Chem. B 109 (2005) 8040.

[47] G. Barcaro, A. Fortunelli, J. Chem. Theory Comput. 1 (2005) 972.
[48] A. Bogicevic, D.R. Jennison, Surf. Sci. 515 (2002) L481.
[49] I. Yudanov, G. Pacchioni, K. Neyman, N. Rösch, J. Phys. Chem. 101 (1997) 2786.
[50] K.M. Neyman, C. Inntam, V.A. Nasluzov, R. Kosarev, N. Rösch, Appl. Phys. A 78 (2004) 823.
[51] N. Lopez, F. Illas, N. Rösch, G. Pacchioni, J. Chem. Phys. 110 (1999) 4873.
[52] G. Pacchioni, P. Pescarmona, Surf. Sci. 412–413 (1998) 657.
[53] K.M. Neyman, D.I. Ganyushin, A.V. Matveev, V.A. Nasluzov, J. Phys. Chem. A 106 (2002) 5022.
[54] S. Majumder, A.V. Matwev, N. Rösch, Chem. Phys. Lett. 382 (2003) 186.
[55] M. Atanasov, C.A. Daul, C. Rauzy, Struct. Bond. 106 (2004) 97.
[56] M. Atanasov, E.J. Baerends, P. Baettig, R. Bruybdockx, C. Daul, C. Rauzy, M. Zibiri, Chem. Phys. Lett. 399 (2004) 433.
[57] F. Neese, J. Chem. Phys. 122 (2005) 034107.
[58] P.H. Kasi, D. McLeod, J. Chem. Phys. 55 (1971) 1566.